Towards a behavior analysis of remote-sensed vessels

Marco Reggiannini, Emanuele Salerno, Massimo Martinelli, Marco Righi, Marco Tampucci and Luigi Bedini
Institute of Information Science and Technologies
National Research Council of Italy
Pisa, Italy
Email: {marco.reggiannini, emanuele.salerno, massimo.martinelli, marco.righi, marco.tampucci, luigi.bedini}@isti.cnr.it

***Abstract*—This paper analyzes the potentialities to classify vessels detected through optical and synthetic-aperture radar (SAR) satellite-borne platforms and estimate their motion. For classification, the discriminative power of a set of geometric features extracted from segmented remote-sensed images is evaluated by clustering data derived from a set of accurate footprints belonging to either tanker or cargo ships. The same procedure is repeated on a few dozens of real, remote-sensed optical images. Concerning velocity estimation, which in this context is based on the detection and analysis of the wake pattern generated by the ship motion, a discussion concerning the accuracy of the wake detection task is presented. In particular, since wake patterns are usually hard to detect, a method is proposed to enhance the wake signal-to-noise ratio, based on a dedicated pre-filtering stage. Results returned by the proposed method are compared with those obtained adopting a standard literature approach, eventually observing that the introduction of the pre-filtering stage improves the wake detection accuracy. A maritime surveillance system based on a pipeline of the modules described here represents a useful tool to support the authorities in charge of monitoring maritime traffic with safety, security and law enforcement purposes.**

***Index Terms*—maritime awareness system, sea surveillance, SAR sensing, optical sensing, image segmentation, image classification, wake detection and analysis**

I. Introduction

Maritime surveillance is of vital importance in safety and security applications, including safety of life at sea, marine traffic control, and monitoring of smuggling and other illegal activities [1], [2]. High-resolution, satellite-borne SAR, is one of the technologies of choice in this field, as it provides wide-area images independent of weather and daylight. Optical images from satellite platforms, when available, are also useful for their higher resolution and their capability of revealing otherwise unobservable details and behaviors. Thus, an integrated use of satellite data, along with additional information from collaborative vessels, enable the designated authorities to monitor a large number of targets at once. To discover anomalous behaviors among possibly hundreds of vessels and take the appropriate countermeasures in due time, however, such authorities cannot rely on human operators alone: a partially or fully automatic analysis system that is able to detect all the ships in the imaged area is essential. This is why, for years, the focus of SAR image analysis for maritime surveillance has been maintained on fast and automatic ship detection, leading to the *de facto* standard method of constant false-alarm ratio (CFAR, see [3], [4]) and some other methods, such as [5]–[7].

This paper describes accuracy issues concerning two specific software procedures dedicated to sea surveillance, namely the classification of seagoing vessels and the estimation of their kinematics. These tasks can be considered as part of a sequential chain of procedures, each addressing a specific aim oriented to the extraction of meaningful information. The classification task takes as input the output of a ship detection stage, i.e. submaps extracted from the input images, each cropped so to only contain a single target. Each submap is fed to a ship segmentation module in charge of refining the identification of the target footprint. Further processing provides additional information concerning the target, such as its length overall, beam overall and heading (possibly up to a 180° ambiguity), as well as other geometric and scatterometric features. These features can then be fed to a ship classification module. Different feature sets extracted from the same data clearly affect the discriminative capability of a classifier. This represents a relevant issue in maritime monitoring, due to the large variability of the target appearances in the imagery employed. In the last few years, a promising answer to these issues seems to be provided by Convolutional Neural Networks (CNN) [8], which improve the capability to identify and classify multimedia data in general. A number of works have been published to evaluate the use of CNN in vessel identification and classification [9]. The main issue with this strategy is always to collect a large, properly annotated image data set. This is not a common possibility in maritime monitoring, especially when SAR images are needed. This is why, for the time being, we are limiting our investigation to the performances that can be obtained from predefined features, leaving apart deep learning approaches.

Along with the estimated class, the estimated kinematics of a ship can be exploited to predict her behavior, which increases the amount of knowledge useful for subsequent, finer processing stages, such as possibly non-collaborative vessel identification. In her motion through the water, a ship generates a wake, whose peculiar visual features depend directly on the vessel velocity. By detecting the linear envelopes of the main wake components and performing a frequency analysis of their observable oscillations, it is possible to estimate univocally the heading and the velocity module of the ship.

The rest of the paper is arranged as follows: Section II presents a brief overview of the state of the art concerning ship classification and ship motion estimation, Section III describes the procedure of ship footprint segmentation followed by the extraction of the geometrical features, Section IV presents an analysis about the discriminative power of the extracted features, Section V concerns the ship kinematics estimation issue and provides an analysis of the wake detector accuracy by comparing the proposed method with a standard literature approach. Some future prospects are finally discussed in Section VI.

II. Related Work

In the last decade, several classification approaches have been attempted, based on different sets of geometrical, scatterometric (see [10]–[15]) or polarimetric (see [16]–[21]) features, and exploiting theoretical scattering models or machine learning on labeled training data to relate the feature vectors to the ship classes. Of course, the availability and reliability of discriminative features depends on the type and the quality of the images analyzed. Previous literature assessed that the only features relevant to both medium-to-high resolution, single-polarization SAR and optical images are either geometrical, derived from length/area measurements, or spatial statistics such as textures, etc. As far as the scatterometric features are concerned, SAR allows us to compute radar-cross-section histograms over either the whole ship footprint or selected parts thereof. A classifier specific for high-resolution optical images can also be based on morphological features extracted from possibly recognizable parts of the ship structure. Actually, for a surveillance system that uses heterogeneous data from several sensors and services, it would be desirable to avoid specific strategies for different types of data.

For this reason, although we are extracting scatterometric features from the SAR images at our disposal, we are still trying to implement an effective classifier that only accepts size and shape features. This would allow us to treat optical and SAR images in the same way and to distinguish between a few major ship classes, provided that an accurate detection and segmentation system is available [22]. In [23], we proposed a segmentation method for both optical and SAR ship images that starts from a detection output supposed to contain a single ship and finds a refined estimate of the ship footprint along with an enclosing rectangle providing gross length and width estimates.

Several methods have been proposed to deal with the issue of estimating the ship motion from SAR imagery. An accurate description of the physics underlying the wake pattern produced by ships moving through the water is long available [24]. Such a pattern is directly related to the velocity of the vessel over the sea surface, and is mapped in SAR images by features related, in turn, to the velocity vectors (over ground) of both the vessel and the sensor platform. Since the wake morphological features are directly related to the ship motion [25], [26], a popular approach to kinematics estimation consists in detecting and later analysing the wake pattern generated by the ship. Wake patterns appear mainly as V-shaped forms, therefore many have proposed wake detectors based on the preliminary recognition of the linear envelopes observed in the wake shape. Zilman et al. [27] proposed a method based on the fast discrete Radon transform to detect the linear segments that start from the wake tip and develop along the wake shape. A similar approach has been adopted by Eldhuset [3], who introduced an approximated Radon transform based on the Chebyshev polynomials. In this way, the detector performance improves in reliability and robustness against false alarms. Once the linear envelopes of the main wake components have been detected, the backscattered signal can be analysed to extract relevant information. In particular it is possible to estimate, according e.g. to [28]–[30], heading and velocity by a proper analysis of the signal variations observed within the detected linear regions.

III. Ship segmentation and feature extraction

In [23], we proposed a method to obtain a ship footprint and an enclosing rectangle from an SAR or optical image containing a single vessel detected by a CFAR module. Compared to the CFAR output, the estimated footprint provides a refined estimate of the shape, the barycentre and the bearing (possibly up to $180°$) of the target vessel. These estimates are passed to the velocity estimation module for its purposes. The vessel footprint is also used to extract the geometric features for classification. From the SAR profile within the footprint, a set of scatterometric features is also extracted. Since we are trying a unified processing for both optical and SAR images, for the time being, we do not address the discriminative power of the scatterometric features extracted.

Let us now introduce the features we use for our evaluation. Of course, the shape parameters alone are not much discriminative with respect to the possible vessel classes: some absolute metric evaluation is essential, as being large or small can well exclude the membership of a vessel to some specified class. This means that we assume that the pixel size in the input image is known, and uniform all over each image to be treated. In accordance with [31], the basic geometric features we consider are the length and the width overall L and W, the perimeter P and the area A, which can be computed in pixels and then transformed in metric quantities through the known pixel size. L and W can be evaluated from either the enclosing rectangle or the footprint, P from the footprint boundary, and A through the number of pixels in the footprint. These and four additional, derived features are summarized in Tab. I along with their strict and naïve definitions. All the naïve-defined features only derive from L and W, which, in this case, are the only basic features. In principle, then, the strictly-defined features are more informative than the naïve-defined ones, but the problem of establishing whether the former are really more discriminative than the latter is still open, for a twofold motivation: first, the four strictly-defined basic quantities are not mutually independent and, second, depending on the resolution and quality of the input image, the estimation accuracy of the features is not guaranteed, so

TABLE I
GEOMETRIC FEATURES CONSIDERED, AFTER [31].

Feature	Symbol	Strictly-def.	Naïve-def.
Length	L	L	L
Width	W	W	W
Perimeter	P	P	$2(L+W)$
Area	A	A	LW
Elongatedness	Elong	A/W^2	L/W
Aspect ratio	AspRat	W/L	W/L
Circularity	Circ	$4\pi A/P^2$	$4LW/(L+W)^2$
Compactness	Comp	$P/(2\pi L)$	$(L+W)/L$

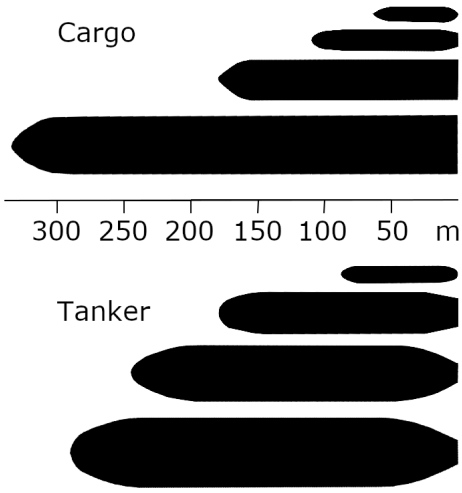

Fig. 1. Samples from the two classes considered in this study (to scale). Top: four footprints of cargo ships (including bulk and container carriers). Bottom: four footprints of tankers (including oil and gas carriers).

the actual discriminative power of the two groups of features could well be equivalent. We assess below this problem by both accurate footprints of real cargo or tanker ships and from satellite-borne optical images.

IV. CLASSIFICATION

We start our analysis of the spaces generated by the features in Tab. I by manually extracting the accurate footprints from 56 high-resolution nadiral ship images, 28 belonging to the class Cargo (either bulk or container ships) and 28 belonging to the class Tanker (either oil or gas carriers), of different sizes. Fig. 1 shows some samples from these sets. To analyze the strictly-defined features, we first show the pairwise scatterplots in Fig. 2.

Apparently, the four basic quantities are strictly correlated; they are less correlated with the derived quantities. Among the latter, Elongation, Aspect Ratio and Circularity are clearly mutually correlated, whereas Compactness seems to be less correlated with all the remaining features. Visually, these plots do not show the presence of any relevant cluster. This means that no single pair of these features is able to discriminate effectively between the two ship classes considered. The next

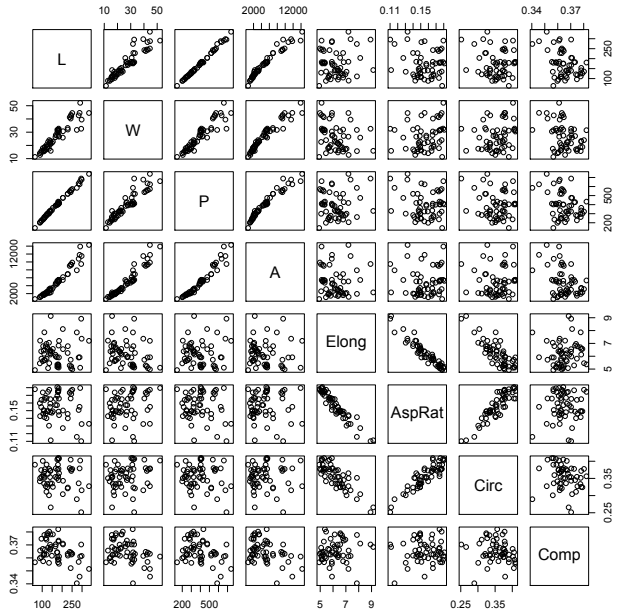

Fig. 2. Pairwise scatterplots of the 8 strictly-defined geometric features in Table I (original coordinates).

step is to assess the information content of the selected features. We do this through a principal component analysis (PCA) of the normalized feature values: each feature set is first normalized to have unit variance and then fed to the PCA routine. The result is shown in Tab. II. As can be seen, the first five principal components have standard deviations within one order of magnitude; the standard deviations 6, 7 and 8 are one order of magnitude smaller. The first principal component is affected almost equally by L, W, P, A and Comp; the weights of the remaining features are at least one order of magnitude below. The second component is mainly affected by Elong, AspRat and Circ; the third component is almost totally covered by Comp; the fourth component is mainly affected by Circ and Elong, and the fifth component is again dominated by the four basic features L, W, P and A.

The same analysis can be performed on the naïve-defined features in Tab. I. The pairwise scatterplots are shown in Fig. 3. In this case, there are only two basic features, and it is to be noted that Elong, AspRat, Circ and Comp are perfectly correlated to each other, as each of them is just a function of any of the others. The standard deviations and the eigenvectors resulting from the PCA are detailed in Tab. III. The last two columns of the PC matrix are not shown since the related eigenvalues have orders of magnitude 10^{-15} and 10^{-16}, respectively. Adopting the same criterion as before, the dominant principal components are now 4. Note that all the features affect about equally the first two components, whereas the first four features have almost no influence in the sixth component. From a comparison between the results in Tabs. II and III, it is confirmed that the strictly-defined features contain

TABLE II
STRICTLY-DEFINED FEATURES: STANDARD DEVIATIONS AND PRINCIPAL COMPONENT MATRIX.

Sdev	2.016	1.694	0.921	0.421	0.137	0.096	0.081	0.015
	PC1	PC2	PC3	PC4	PC5	PC6	PC7	PC8
L	-0.4886	0.0849	-0.0819	-0.0006	-0.2849	0.3788	-0.0579	0.7205
W	-0.4777	-0.1242	-0.1547	-0.0032	-0.2458	-0.8195	-0.0157	0.0054
P	-0.4847	0.0881	-0.1492	-0.0018	-0.3251	0.3905	-0.0048	-0.6904
A	-0.4908	-0.0006	-0.0820	-0.0742	0.8611	0.0424	0.0556	-0.0194
Elong	0.0291	0.5661	0.0240	-0.6419	-0.0633	-0.0953	0.5023	0.0206
AspRat	0.0118	-0.5815	-0.1626	0.0829	-0.0573	0.1140	0.7814	0.0384
Circ	-0.0079	-0.5557	0.117	-0.7496	-0.0421	0.0884	-0.3246	-0.0166
Comp	0.2366	0.0443	-0.9484	-0.1160	0.0444	0.0248	-0.1579	0.0390

TABLE III
NAÏVE-DEFINED FEATURES: FIRST 6 STANDARD DEVIATIONS AND PRINCIPAL DIRECTIONS.

Sdev	2.025	1.963	0.145	0.122	0.088	0.003
	PC1	PC2	PC3	PC4	PC5	PC6
L	-0.2683	0.4263	-0.3205	0.0369	0.4620	-0.0017
W	-0.1035	0.4963	-0.1718	0.2503	-0.8003	0.0010
P	-0.2484	0.4394	-0.3032	0.0659	0.2960	-0.0014
A	-0.1903	0.4657	0.8030	-0.3165	0.0420	0.0029
Elong	-0.4566	-0.1863	-0.2864	-0.7547	-0.2307	0.2276
AspRat	0.4502	0.2076	-0.1535	-0.3588	-0.0091	-0.3190
Circ	0.4531	0.2021	-0.0416	-0.0653	0.0563	0.8629
Comp	0.4502	0.2076	-0.1535	-0.3588	-0.0091	-0.3190

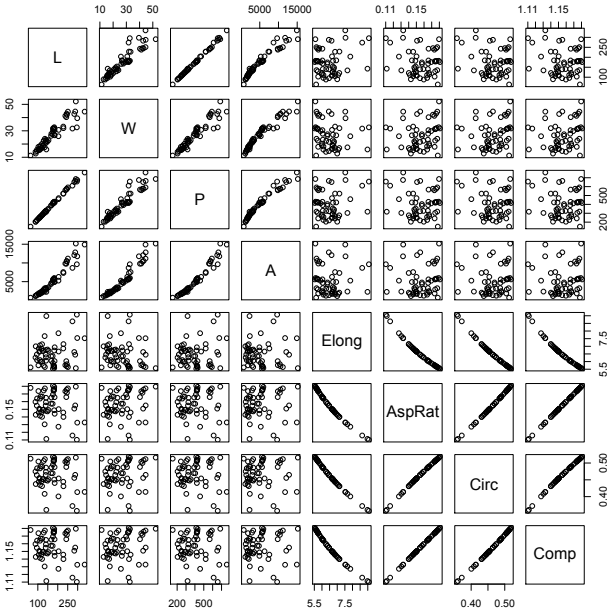

Fig. 3. Pairwise scatterplots of the naïve-defined geometric features in Table I (original coordinates).

more independent information than the naïve-defined features. However, we computed the features from accurate footprints of the type in Fig. 1. Thus, this observation can be considered conclusive with high-resolution, low-clutter SAR and optical images.

We attempted a binary clustering of all the available data, and report here the results obtained by the `clara` clustering algorithm [32], implemented in the R `cluster` package. The results using the euclidean metric to compute the dissimilarities are shown graphically in Figs. 4 and 5. The first cluster computed from the strictly defined features contains 15 tankers and 3 cargo ships; the second cluster contains 13 tankers and 25 cargo ships. The corresponding results from the naïve features are, in cluster 1, 16 tankers and 7 cargo, and, in cluster 2, 12 tankers and 21 cargo ships. Assuming that some classification algorithm has labeled the targets in clusters 1 and 2, respectively, as "Tanker" and "Cargo", Tab. IV shows the classification performance indices obtained through the strictly-defined and the naïve-defined geometric features (SGF and NGF, respectively).[1] Overall, the strictly-defined features seem to be slightly more performant than the naïve ones. This is confirmed by the values of the F1-score. Note also, from Fig. 5, that the first two components of the NGF set explain a 99.45% of the variability. This means that only using those two components in classification should be nearly equivalent to using the whole feature set. Again, the slightly superior performance of the SGFs over the NGFs using this clustering method does not justify a choice in favor of one of these sets, independently of the actual classification strategy adopted with

[1]Equivalently, the two classes could be named "Tanker" and "non-Tanker", thus justifying, respectively, what we considered the "Positive" and "Negative" outputs to build Tab. IV following the standard definitions of the performance indices (see [33], or https://en.wikipedia.org/wiki/Precision_and_recall, last checked 28 October 2019).

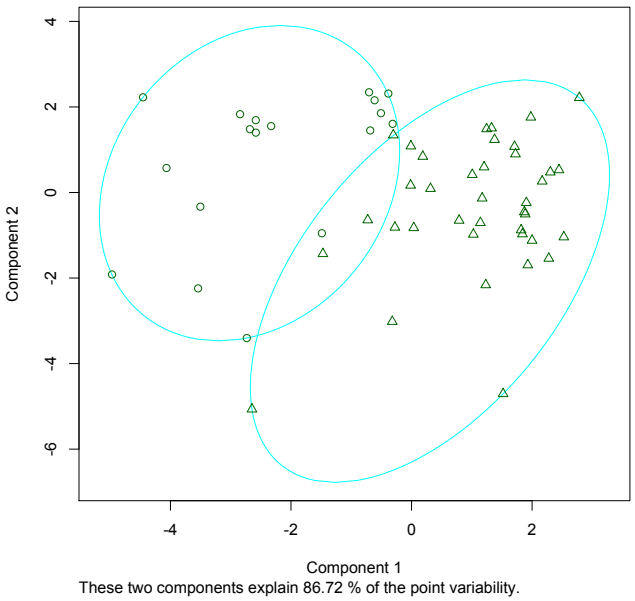

Fig. 4. `clara` cluster plots projected onto the first two components, from strictly-defined features.

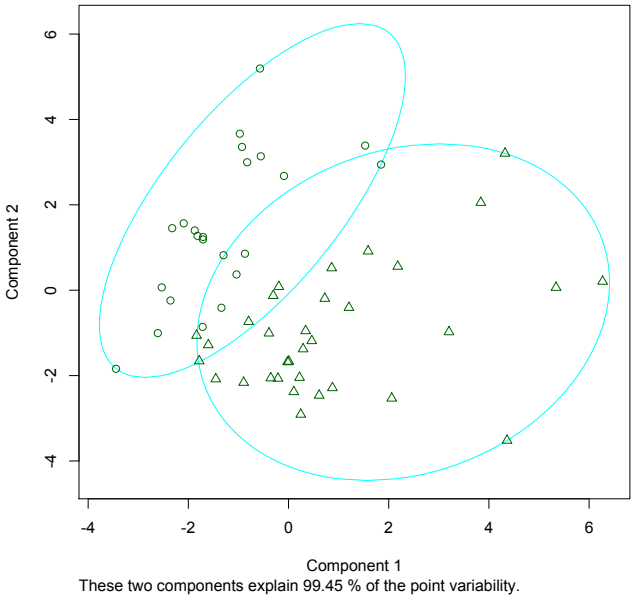

Fig. 5. `clara` cluster plots projected onto the first two components, from naïve-defined features.

the real data.

Typical pixel sizes of our 56 accurate footprints are in the range $10 \div 20$ cm. For both the feature types considered, the medoids of the two clusters provided by `clara` have been used as references for the features evaluated on a real dataset

TABLE IV
CLASSIFICATION PERFORMANCE INDICES FROM THE TWO FEATURE SETS.

Index \ Feature set	SGF	NGF
Sensitivity	0.536	0.571
Specificity	0.893	0.750
Precision	0.833	0.696
Negative Predictive Value	0.658	0.636
Accuracy	0.714	0.661
F1-Score	0.652	0.627

TABLE V
CLASSIFICATION PERFORMANCE INDICES FOR THE EROS-B TEST SET.

Index \ Feature set	SGF	NGF
Sensitivity	0.594	0.594
Specificity	1.	0.692
Precision	1.	0.704
Negative Predictive Value	0.667	0.581
Accuracy	0.776	0.638
F1-Score	0.745	0.644

extracted from EROS-B[2] images. We selected 58 footprints (32 tankers and 26 cargo ships with typical pixel sizes of about 1 m) and measured the euclidean distances of the individual features from the above-mentioned medoids. Out of the 32 tankers, 19 were classified correctly and 13 were misclassified. All the 26 cargo ships were classified correctly. The related performance indices are shown in Tab. V for both the feature sets. Again, and more apparently than before, the performance obtained through the strictly-defined features is better than the one obtained through the naïve-defined features. Note that the accuracy from the SGFs is more than a 77% and the accuracy from the NGFs is less than a 64%.

It is also to note that the features extracted from the EROS-B optical images are almost as accurate as the ones extracted from the high-definition images used in Section IV, despite the significant differences in pixel sizes. Nevertheless, as argued in [31], lower-resolution images, or artifacts or systematic errors, could well diminish the advantages of the SGFs over the NGFs. This could be the case with SAR data.

In Fig. 6 the footprints of the 13 false negatives from the test data set (misclassified tankers), using the SGFs, are shown. Except for the three medium-sized vessels, these are all small oil products tankers with lengths of 100 m or less. Since, in average, the cargo ships in this dataset are smaller than the tankers, this could suggest that the most important feature is actually the length overall. This is not true since the two length ranges significantly overlap, and there are many correctly classified cargo ships comparable in length to the tankers (up to 225 m).

V. KINEMATICS ESTIMATION

Satellite imagery provides single instantaneous information about the traffic circumstance within a given area of interest.

[2]https://directory.eoportal.org/web/eoportal/satellite-missions/e/eros-b, last checked 28 October 2019

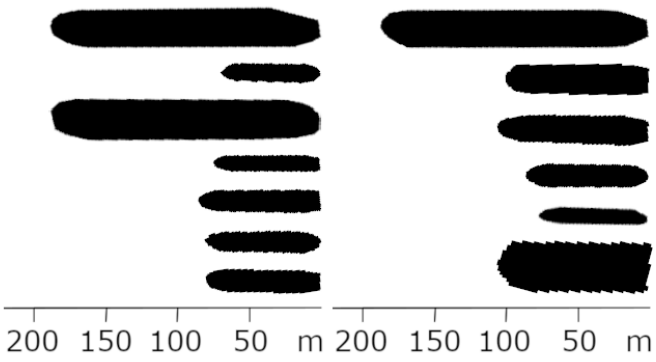

Fig. 6. Misclassified tanker footprints from the set used for Tab. V (to scale).

In case the corresponding velocity information is known, route and future behavior of the detected vessels can be predicted through proper machine learning algorithms. For this reason the capability to extract information about the ship kinematics from remote sensing imagery is of paramount relevance to maritime monitoring. Here, we refer to a kinematics estimation module based on image processing. The proposed module applies a wake detector to the input image and exploits the detected pattern to estimate the vessel's velocity.

The wake pattern is a combination of multiple oscillatory components, whose summation exhibits a V-shaped envelope centered on the ship route axis. Its angular aperture is approximately 39°. Exploiting these observable phenomena, the route direction can be estimated by first detecting the V pattern (Fig. 7) through a Radon-transform-based linear detector [34], and then identifying the wake center axis. Once the wake pattern has been recognized, its internal components can be analyzed to extract features that enable to estimate the ship kinematics. To this purpose, relevant features related to the motion of the ship are (i) the displacement between the vessel target and the wake tip, called Azimuth shift (only observed in SAR), and (ii) the spatial wavelength of the plane wave oscillation located at the edge sector of the wake envelope (*Kelvin wake*).

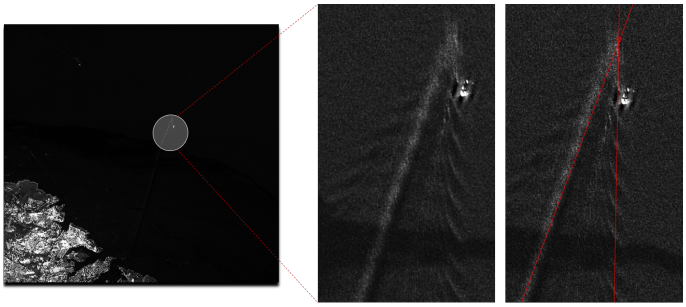

Fig. 7. Wake pattern detection.[3]

Unfortunately, ship wakes are not always visible or too faint to be detected. Typically, due to very low Signal-to-Noise Ratios, wake detection is a task with a very small probability of success. Different approaches have been proposed (see e.g. [35], [36]) to improve the poor results obtained through classical methods, e.g., based on the straightforward application of the Radon/Hough transform on intensity images. Taking inspiration from [3], [37], a novel method has been proposed for detecting and analysing wake patterns through SAR map processing [38]. First, the gradient of the input image is computed by means of a dedicated procedure, following an approach specifically suited for speckle-affected data, such as SAR images. Assuming that the linear envelopes of the central/peripheral wake sectors are the main observable wake features in SAR maps, the estimated gradient feeds an algorithm based on the Radon transform, whose goal is to detect those segments. Eventually, the algorithm returns a decision statement about the presence of a wake pattern. This final decision is put forward according to the specific arrangement of the detected linear segments. In case of a positive detection, the corresponding wake pattern is identified and its relevant features are employed to estimate route and speed parameters of the ship. Further details about the gradient based wake detector can be found in [39].

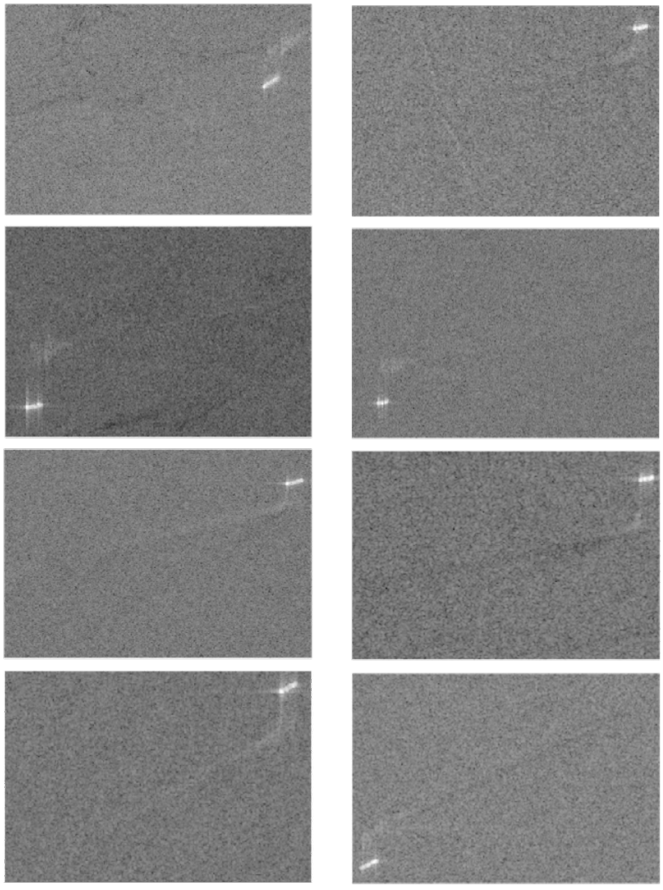

Fig. 8. Dataset employed to test the turbulent wake detector (contains modified Copernicus Sentinel data, 2018).

The described wake detector has been applied to the dataset of Sentinel-I imagery samples illustrated in Fig. 8.

An evaluation of the proposed method has been performed by comparing the obtained results with those returned by the method proposed in [3]. The corresponding error plots are shown in Figs. 9 and 10, where the estimated Azimuth displacement and turbulent wake orientation have been plotted versus the corresponding true values. Fig. 9 gives the comparison between true and estimated data when the latter have been obtained directly from the intensity maps, while Fig. 10 refers to our strategy of preprocessing the intensity map as in Section V. The improved performance of our strategy is apparent by comparing the two figures.

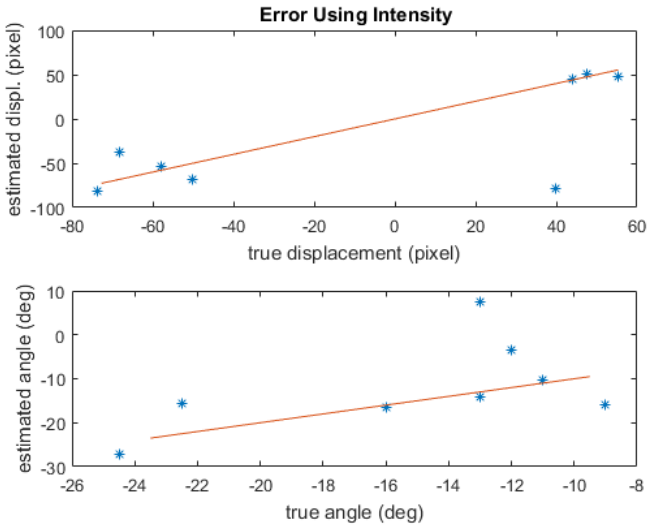

Fig. 9. Method proposed in [3], error diagram.

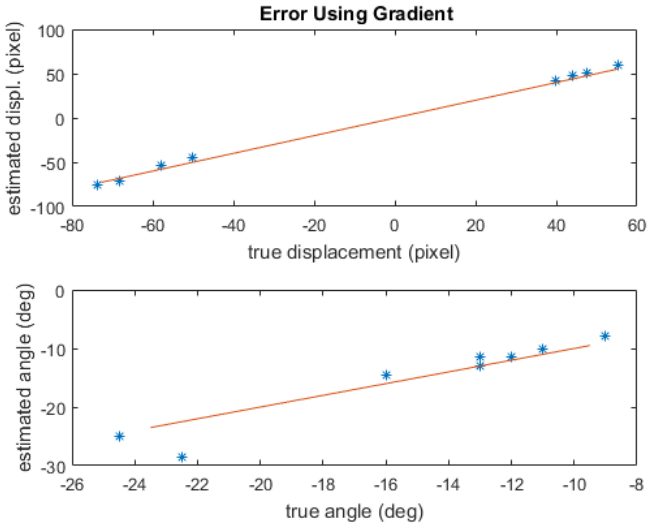

Fig. 10. Method proposed here, error diagram.

VI. Conclusions

This document addresses different accuracy issues concerning two crucial processing stages integrated inside a typical maritime surveillance system. First of all, the authors discuss the discriminative power of a given set of geometric features in view of a classification of tanker and cargo ships. The analysis performed demonstrates how deriving the features from their strict definitions potentially provides a discriminative power that is better than that obtained by using the corresponding naïve definitions. A more conclusive result about the practical usefulness of the features considered would need an analysis of a larger data set, with a broader range of geometric estimation errors, such as the ones often found in SAR imagery.

Then, concerning a processing stage dedicated to the estimation of the kinematics of a detected vessel, the authors develop a comparative analysis based on the estimation of meaningful motion quantities. The computation has been carried out following a standard literature approach and also adopting a novel method, based on the introduction of a proper gradient filtering in the preliminary stages of the module. Promising results obtained by processing the dataset in Fig. 8 suggest that employing the proposed gradient-based approach may enhance the accuracy concerning the estimation of the ship motion's related features (see charts in Figs. 9 and 10).

Concerning future prospects, the authors envisage the development of novel procedures for wake detection, taking inspiration from cutting edge literature of machine learning. To this purpose, particular interest will be devoted to deep convolutional networks, employed as powerful tools for the extraction of discriminating features from large amounts of open access data (e.g., the ESA Copernicus Open Access Hub). Wake patterns are hardly detectable in SAR maps, hence future developments will also be devoted to the refinement of the wake recognition process, based on the exploitation of additional information, such as the fine estimate of the vessel position as well as the constraints of this peculiar hydrodynamics problem, e.g. the theoretically expected wake angular aperture. For what concerns velocity estimation, novel methods are currently being investigated to evaluate their potential in terms of kinematics information extraction. In particular, along-track-interferometry techniques represent interesting tools for the purpose of estimating the line-of-sight velocity value through the analysis of single-look-complex SAR data. Moreover, the Doppler centroid of the SAR signal varies according to the kinematics of the scatterer. Estimating the variation between the Doppler centroid of a moving object w.r.t. a stationary one provides an additional velocity estimation method, which sounds worth being further studied.

References

[1] "Examining the creation of a european border surveillance system (eurosur)," Tech. Rep. 52008SC0151, European Commission, https://eur-lex.europa.eu/legal-content/EN/TXT/?qid=1529409655955&uri=CELEX:52008SC0151, 2008.

[2] E. Shahbazian *et al.*, Ed., *Harbour Protection Through Data Fusion Technologies*, Springer Science + Business Media B.V, 2009.

[3] K. Eldhuset, "An automatic ship and ship wake detection system for spaceborne sar images in coastal regions," *IEEE Trans. Geosci. Remote Sens.*, vol. 34, pp. 1010–1019, 1996.

[4] D. J. Crisp, "The state-of-the-art in ship detection in synthetic aperture radar imagery," Report DSTO-RR-0272, Australian Government, Department of Defence, May 2004.

[5] M. Tello, C. López-Martínez, and J. J. Mallorqui, "A novel algorithm for ship detection in sar imagery based on the wavelet transform," *IEEE Geosci. Remote Sens. Lett.*, vol. 2, pp. 201–205, 2005.

[6] M. Messina, M. Greco, L. Fabbrini, and G. Pinelli, "Modified otsu's algorithm: a new computationally efficient ship detection algorithm for sar images," in *2012 CNIT Tyrrhenian Workshop*. 2012, pp. 262–266, IEEE.

[7] M. Sugimoto, K. Ouchi, and Y. Nakamura, "On the novel use of model-based decomposition in sar polarimetry for target detection on the sea," *Remote Sens. Lett.*, vol. 4, pp. 843–852, 2013.

[8] Y. LeCunn, Y. Bengio, and G. Hinton, "Deep learning," *Nature*, vol. 521, pp. 436–444, 2015.

[9] J. Tang, C. Deng, G. Huang, and B. Zhao, "Compressed-domain ship detection on spaceborne optical image using deep neural network and extreme learning machine," *IEEE Transactions on Geoscience and Remote Sensing*, vol. 53, no. 3, pp. 1174–1185, 2015.

[10] X. Tian, C. Wang, H. Zhang, and F. Wu, "Extraction and analysis of structural features of ships in high-resolution sar images," in *Proc. IEEE CIE Intl. Conf. on Radar*, 2011, pp. 630–633.

[11] G. Margarit and A. Tabasco, "Ship classification in single-pol sar images based on fuzzy logic," *IEEE Trans. Geosci. Remote Sens.*, vol. 49, pp. 3129–3138, 2011.

[12] X. Xing, K. Ji, H. Zou, W. Chen, and J. Sun, "Ship classification in terrasar-x images with feature space based sparse representation," *IEEE Geosci. Rem. Sens. Lett.*, vol. 10, pp. 1562–1566, 2013.

[13] H. Lang, J. Zhang, X. Zhang, and J. Meng, "Ship classification in sar image by joint feature and classifier selection," *IEEE Geosci. Remote Sens. Lett.*, vol. 13, pp. 212–216, 2016.

[14] S. Jiang, C. Wang, H. Zhang, F. Wu, and B. Zhang, "Civilian ship classification based on structure features in high resolution sar images," *Proc.SPIE*, vol. 8525, pp. 852505 1–7, 2012.

[15] M. Jiang, X. Yang, Z. Dong, S. Fang, and J. Meng, "Ship classification based on superstructure scattering features in sar images," *IEEE Geosci. Remote Sens. Lett.*, vol. 13, pp. 616–620, 2016.

[16] R. Touzi, F. J. Charbonneau, R. K. Hawkins, and P. W. Vachon, "Ship detection and characterization using polarimetric sar," *Can. J. Remote Sens.*, vol. 30, pp. 552–559, 2004.

[17] G. Margarit, J. J. Mallorqui, and X. Fàbregas, "Single-pass polarimetric sar interferometry for vessel classification," *IEEE Trans. Geosci. Remote Sens.*, vol. 45, pp. 3494–3502, 2007.

[18] G. Margarit, J. J. Mallorqui, J. Fortuny-Guasch, and C. Lopez-Martinez, "Exploitation of ship scattering in polarimetric sar for an improved classification under high clutter conditions," *IEEE Trans. Geosci. Remote Sens.*, vol. 47, pp. 1224–1235, 2009.

[19] Y. Allard, M. Germain, and O. Bonneau, "Ship detection and characterization using polarimetric sar data," in *[2]*, pp. 243–250.

[20] M. Martorella, E. Giusti, A. Capria, F. Berizzi, and B. Bates, "Automatic target recognition by means of polarimetric isar images and neural networks," *IEEE Trans. Geosci. Remote Sens.*, vol. 47, pp. 3786–3794, 2009.

[21] H. Lang, J. Zhang, T. Zhang, D. Zhao, and J. Meng, "Hierarchical ship detection and recognition with high resolution polarimetric synthetic aperture radar imagery," *J. Appl. Remote Sens.*, vol. 8, no. 083623, 2014.

[22] M. Stasolla, J. J. Mallorqui, G. Margarit, C. Santamaria, and N. Walker, "A comparative study of operational vessel detectors for maritime surveillance using satellite-borne synthetic aperture radar," *IEEE J. Sel. Top. Appl. Earth Obs. Remote Sens.*, vol. 9, pp. 2687–2701, 2016.

[23] L. Bedini, M. Righi, and E. Salerno, "Size and heading of sar-detected ships through the inertia tensor," *Proceedings (MDPI)*, vol. 2, no. 97, 2018.

[24] W. Thomson, "On the waves produced by a single impulse in water of any depth, or in a dispersive medium," *Proc. R. Soc. Lond.*, vol. 42, pp. 80–83, 1887.

[25] E. O. Tuck, S. I. Collins, and W. H. Wells, "On ship wave patterns and their spectra," *J. Ship Res.*, vol. 15, pp. 11–21, 1991.

[26] F. S. Crawford, "Elementary derivation of thewake pattern of a boat," *Am. J. Phys.*, vol. 51, pp. 782–785, 1984.

[27] G. Zilman, A. Zapolski, and M. Marom, "The speed and beam of a ship from its wake's sar images," *IEEE Trans. Geosci. Remote Sens.*, vol. 42, pp. 2335–2343, 2004.

[28] J. K. E. Tunaley, "The estimation of ship velocity from sar imagery," in *Proceedings of the 2003 IEEE International Geoscience and Remote Sensing Symposium*, Toulouse, France, July 2003, pp. 191–193.

[29] A. Scherbakov, R. Hanssen, G. Vosselman, and R. Feron, "Ship wake detection using radon transforms of filtered sar imagery," *Proc. SPIE*, vol. 2958, pp. 96–106, 1996.

[30] M. D. Graziano, M. D'Errico, and G. Rufino, "Ship heading and velocity analysis by wake detection in sar images," *Acta Astronaut.*, vol. 128, pp. 72–82, 2016.

[31] H. Lang and S. Wu, "Ship classification in moderate-resolution sar image by naive geometric features-combined multiple kernel learning," *IEEE Geosci. Remote Sens. Lett.*, vol. 14, pp. 1765–1769, 2017.

[32] L. Kaufman and P. J. Rousseeuw, *Finding Groups in Data: An Introduction to Cluster Analysis*, Wiley, New York, 1990.

[33] D. L. Olson and D. Delen, *Advanced Data Mining Techniques*, Springer, 2008.

[34] R.C. Gonzalez and R.E. Woods, *Digital Image Processing*, Pearson Prentice Hall, Upper Saddle River, NJ, USA, 2008.

[35] M. Krishnaveni, S.K. Thakur, and P. Subashini, "An optimal method for wake detection in sar images using radon transformation combined with wavelet filters," *Int. J. Comput. Sci. Inf. Secur.*, vol. 6, 2009.

[36] F. Chaillan and P. Courmontagne, "On the use of the stochastic matched filter for ship wake detection in sar image," in *Proceedings of the OCEANS 2006*, Boston, MA, USA, September 2006.

[37] S. Song, B. Xu, and J. Yang, "Sar target recognition via supervised discriminative dictionary learning and sparse representation of the sar-hog feature," *MDPI Remote Sens.*, vol. 8, pp. 683, 2016.

[38] M. Reggiannini, "Remote sensing for maritime monitoring and vessel characterization," in *Proceedings of the OCEANS 2019*, Marseille, France, June 2019.

[39] M. Reggiannini and L. Bedini, "Multi-sensor satellite data processing for marine traffic understanding," *Electronics*, vol. 8, pp. 152, 2019.